Electrodeposition of Nickel Hydroxide Nanoparticles on Boron-Doped Diamond Electrodes for Oxidative Electrocatalysis

ARTICLE *in* THE JOURNAL OF PHYSICAL CHEMISTRY C · DECEMBER 2010

Impact Factor: 4.77 · DOI: 10.1021/jp109526b

6 AUTHORS, INCLUDING:

Marcio Vidotti
Universidade Federal do Paraná
41 PUBLICATIONS **638** CITATIONS
SEE PROFILE

Anisha N Patel
Paris Diderot University
13 PUBLICATIONS **259** CITATIONS
SEE PROFILE

Mark Edward Newton
The University of Warwick
105 PUBLICATIONS **1,784** CITATIONS
SEE PROFILE

Julie V Macpherson
The University of Warwick
175 PUBLICATIONS **5,627** CITATIONS
SEE PROFILE

THE JOURNAL OF PHYSICAL CHEMISTRY C

ARTICLE

pubs.acs.org/JPCC

Electrodeposition of Nickel Hydroxide Nanoparticles on Boron-Doped Diamond Electrodes for Oxidative Electrocatalysis

Laura A. Hutton,[⊥,†] Marcio Vidotti,[⊥,§] Anisha N. Patel,[†] Mark E. Newton,[‡] Patrick R. Unwin,[†] and Julie V. Macpherson[†,*]

[†]Departments of Chemistry and [‡]Physics, University of Warwick, CV4 7AL, Coventry, U.K.

[§]Departamento de Química, Universidade Federal do Paraná, CP 19081, CEP 81531-980 Curitiba, PR, Brazil

ABSTRACT: We demonstrate, for the first time, the electrosynthesis of uniformly dispersed nickel hydroxide nanoparticles (NPs) on polycrystalline boron-doped diamond (pBDD). This has been achieved by electrogenerating OH^- at the pBDD surface in the presence of Ni^{2+} to create local conditions near the electrode where highly supersaturated (relative saturation ratio > 10^5) nickel hydroxide solutions are generated for short periods of time (approximately seconds). This results in the deposition of nickel hydroxide NPs directly on the electrode surface, as confirmed by X-ray photoelectron spectroscopy. The NPs have a reasonably homogeneous size distribution and are deposited uniformly across the heterogeneous pBDD surface. We show that by simply increasing the electrogeneration time and, hence, increasing both the local concentration of OH^- and extent of the precipitation reaction, it is possible to increase the size of the NPs. For example, after 1 s, NPs with dimensions of 12 ± 3 nm form, whereas after 15 s, NPs of size ∼39 ± 9 nm result. Longer times result in larger particles, which form aggregated structures. The effect of nickel hydroxide NP size on electrocatalytic activity was investigated by measuring the steady-state current for the oxidation of glucose in alkaline media. For NPs ≥ 25 nm in size, glucose oxidation is close to diffusion-controlled. However, for the smallest NPs produced (∼12 nm) the currents passed suggest kinetic limitations. For glucose at an effective surface coverage of nickel hydroxide of ∼20 nmol cm^{-2}, equivalent to 15 ng of nickel hydroxide, this functionalized electrode showed a sensitivity of 330 μA mM^{-1} cm^{-2} and a limit of detection of 400 nM. The latter represents one of the lowest limits of detection for glucose for nickel hydroxide-based electrodes. The electrocatalytic oxidation properties of this electrode toward methanol and ethanol was also found to be very efficient, yielding very high density currents of ∼1010 A g^{-1} for 0.5 M ethanol and 990 A g^{-1} for 0.47 M methanol.

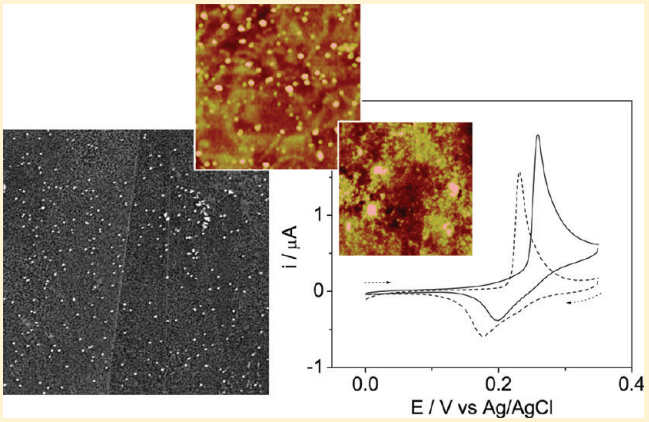

INTRODUCTION

The search for electrocatalytic materials is the focus of intense study in a variety of research areas, such as for fuel cell catalysts, energy storage, chemical synthesis, and electrochemical-based sensors.[1] Among many possible electrocatalytic materials, nickel hydroxide has been the subject of much investigation, particularly as a fuel cell catalyst, for secondary batteries,[2] and as an electrocatalyst for organic synthesis.[3−5] The electrocatalytic effect is considered to arise from unpaired d electrons or empty d orbitals associated with the oxidized form of Ni (NiOOH; i.e., Ni^{3+}), which are available for bond formation with adsorbed species or redox intermediates.[6]

For electrocatalytic applications, it has often been found that by moving from bulk materials to nanosized structures, catalytic activity can be significantly increased.[7] Thus, decorating supporting substrates with isolated nanoparticles (NPs) or nanostructures is a popular strategy to create efficient electrocatalysts.[7−9] Although many chemical routes, such as sonochemistry, sol gel, and solvothermal methods, among others,[10] have been described for the formation of nickel hydroxide on surfaces, these methods typically result in thin film structures.[11,12]

The direct formation of particles in situ on the electrode support of interest represents a simpler alternative to the techniques described above. Furthermore, as amply demonstrated for the formation of immobilized metal nanostructures, judicious choice of electrode potential and time opens up the possibility of controlling the size and coverage of electrodeposited nanostructures.[13] The choice of substrate electrode material, which provides electrical connection to the NPs, is also an important consideration.[7] The properties of the surface must be such that a strong NP−electrode interaction is favored. The background (parasitic) current contribution from the substrate electrode should also, ideally, be negligible in the potential region of interest.

Received: October 4, 2010
Revised: November 29, 2010

   dx.doi.org/10.1021/jp109526b | *J. Phys. Chem. C* XXXX, XXX, 000–000

A substrate electrode with a wide potential window also enables depositions to be carried out free from complications from the evolution of gaseous products from direct solvent/electrolyte electrolysis. Finally, the support electrode should also be stable and inert in the solution of interest, particularly to ensure the physical integrity of the electrode and to avoid the production of chemical species that might poison the electrode and electrocatalyst.

Polycrystalline boron-doped diamond (pBDD) meets many of the requirements cited above. It has generated considerable interest as an electrode material, particularly as a consequence of its very wide potential window in aqueous solution compared with traditional electrodes.[14] Moreover, pBDD is characterized by a very low sensitivity to dissolved oxygen, very low background currents, reduced susceptibility to passivation, and corrosion stability in aggressive media and at elevated temperatures and pressures.[15,16] As such, pBDD represents an extremely interesting electrode platform for the electrochemically driven deposition of nickel hydroxide NPs.

To date, previous studies of nickel hydroxide electrodeposition have focused on two approaches: either (i) the electrochemical generation of a base in the presence of Ni^{2+} to form nickel hydroxide directly,[17]

$$Ni^{2+}(aq) + 2OH^-(aq) \rightarrow Ni(OH)_2(s) \quad (1)$$

or (ii) an indirect approach in which nickel is first electrodeposited,

$$Ni^{2+}(aq) + 2e^- \rightarrow Ni(s) \quad (2)$$

or a nickel metal electrode is employed[18] and the nickel is fully oxidized by potential cycling in base.[19−21] In some cases, it is also possible to form mixtures of nickel hydroxide and metallic nickel due to both processes described in eqs 1 and 2, occurring during electrodeposition.[22]

To the best of our knowledge, there are no reports in the literature that show the production of isolated NPs on an electrode surface via the direct approach; rather, thin film structures tend to be produced. For the indirect approach, there are only limited reports of the formation of predominantly approximately micrometer-sized nickel hydroxide particles.[20,21] Furthermore, because this methodology requires electrodeposition of nickel first (eq 2), heterogeneities in the electroactivity of the electrode surfaces employed result in a heterogeneous surface distribution of particles.[20,23] Thus, the ability to tightly control the surface coverage and particle size, which is particularly problematic for fundamental studies, is lost.

In this work, we demonstrate the formation of randomly isolated nickel hydroxide NPs on a hydrophilic oxygen-terminated pBDD surface. Herein, we use the direct method and bias the electrode at an appropriate potential to potentiostatically increase the local pH of the solution, in the presence of Ni^{2+}, to create very high ($>10^5$) relative saturation ratios[24] for a short period of time (approximately seconds). Under these conditions, we show that it is possible to precipitate nickel hydroxide particles as small as ∼10 nm in height randomly over the heterogeneously electroactive pBDD surface. Longer deposition times (>30 s) lead to aggregated structures. By simply controlling the electrodeposition time, it is possible to change the size of the structures formed. In this way, we are able to create electrocatalytic surfaces to investigate, for the first time, the effect of NP size on the electrocatalytic activity of nickel hydroxide toward methanol, ethanol, and glucose oxidation.

EXPERIMENTAL SECTION

Nickel nitrate (Aldrich), KOH (Aldrich), glucose (Aldrich), methanol, and ethanol were used as received. The pBDD 1 mm diameter macrodisc electrode, insulated in glass, was fabricated as described previously.[9] The pBDD substrates were prepared by Element Six Ltd. (E6 Ltd., Ascot, U.K.) using a commercial microwave plasma CVD process developed in-house. The average boron doping level of this material is about 5×10^{20} atoms cm^{-3}, as determined by secondary ion mass spectroscopy.[25] The pBDD samples were polished by E6 Ltd. to give a 500-μm-thick sample with a roughness of ∼1−2 nm on the surface of individual grains, as measured by atomic force microscopy (AFM).[25] The pBDD, prior to electrode sealing, was acid-cleaned in boiling concentrated H_2SO_4 (98%), supersaturated with KNO_3, which renders the surface oxygen-terminated and hydrophilic.

Platinum and Ag/AgCl wire were used as counter and reference electrodes respectively, in conjunction with a CH Instruments 730A potentiostat. All experiments were performed at room temperature in an air conditioned laboratory. All solutions were prepared from Milli-Q water (Millipore Corp.), resistivity of 18.2 MΩ cm at 25 °C

Nickel hydroxide NPs were synthesized in situ on the pBDD surface from a 10 mM nickel nitrate solution (pH = 6). The precipitation of nickel hydroxide is considered to occur due to the electroreduction of nitrate ions (from the nickel salt) in solution,[26,27]

$$NO_3^- + 7H_2O + 8e^- \rightarrow NH_4^+ + 10\,OH^- \quad (3)$$

resulting in an increase in the local pH. This, in turn, drives the precipitation of $Ni(OH)_2$ on the pBDD surface (solubility product, K_{sp}, of $Ni(OH)_2$ is 5.48×10^{-16} at 25 °C[28]) according to eq 1. To drive the homogeneous nucleation of NPs in solution it is important to (i) produce a high concentration of OH^- to form a highly supersaturated solution[24] and (ii) keep the time scales of production short to avoid NP aggregation. This was achieved by exploring different combinations of applied electrode potential and time. Applying a potential of −1.1 V vs Ag/AgCl for different times (from 1 to 100 s) was found to be the most effective strategy for producing different sized nickel hydroxide NPs on the surface.

High resolution characterization of the nickel hydroxide NP-pBDD composite electrode utilized field-emission scanning electron microscopy (FE-SEM), X-ray photoelectron spectroscopy (XPS), and AFM. For these studies, the pBDD columns were fabricated as above and annealed to a flat quartz disk that had also been sputtered with a Ti/Au contact. A conducting wire was adhered to the Au contact of the quartz using silver epoxy. Epoxy resin (Araldite, Bostik Findley, UK) was used to seal around the edges of the pBDD column and the quartz so that only the 1 mm diameter pBDD disk was left uninsulated and exposed to the nickel nitrate solution for electrodeposition.

FE-SEM images were recorded using a secondary electron detector at 3 kV (Zeiss Supra55VP), which allowed the diamond grain morphology and $Ni(OH)_2$ NPs to be imaged simultaneously.

XPS chemical analysis was performed with a Scienta ESCA300 spectrometer at the National Centre for Electron Spectroscopy and Surface Analysis, Daresbury Laboratory, U.K. The samples were probed using a monochromated rotating anode Al Kα X-ray source and analyzed by a 300 mm radius hemispherical analyzer with a slit width of 0.8 mm at a pass energy of 150 eV.

dx.doi.org/10.1021/jp109526b |J. Phys. Chem. C XXXX, XXX, 000–000

AFM images were recorded in tapping mode in order to minimize distortion or possible dragging of the NPs (Veeco Enviroscope AFM with Nanoscope IV controller).

RESULTS AND DISCUSSIONS

Surface Characterization of Nickel Hydroxide-Modified Electrodes. We first consider simple CV measurements of the modified electrodes, which allow an estimation of the amount of electroactive nickel hydroxide on the electrode surface. Figure 1 shows a typical CV recorded in 0.1 M KOH at 5 mV s^{-1} for a nickel hydroxide-modified pBDD electrode produced using a deposition time of 5 s (procedure outlined above). As the potential is scanned more positive, the current increases due to oxidation of Ni^{2+} ($Ni(OH)_2$) to Ni^{3+} (NiOOH).

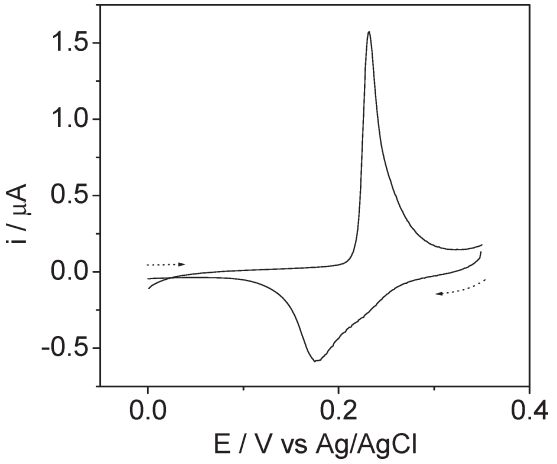

Figure 1. Typical CV recorded in 0.1 M KOH only for a nickel hydroxide modified ($\Gamma \sim 20$ nmol cm^{-2}) pBDD. The scan rate is 5 mV s^{-1}.

$$Ni(OH)_2 + OH^- \leftrightarrow NiOOH + H_2O + e^- \quad (4)$$

Calculation of the charge associated with oxidation (Q_{ox}) of $Ni(OH)_2$ and subsequent reduction (Q_{red}) of the electrogenerated NiOOH gives a value for Q_{ox}/Q_{red} of ~1. The amount of deposited nickel hydroxide can be calculated as an effective surface concentration, Γ, on the electrode surface,

$$\Gamma = Q_{ox}/nFA \quad (5)$$

where F is the Faraday constant (96 485 C mol^{-1}), n is the number of electrons transferred in the redox process ($n = 1$), and A is the geometric area of the pBDD electrode. In this potential window, background contributions from the pBDD electrode are negligible.

Morphological Characterization of the Nickel Hydroxide Modified Electrodes. FE-SEM and AFM were used to characterize the surface of the $Ni(OH)_2$-modified pBDD electrodes. Figure 2 shows typical FE-SEM images for the modified electrodes for Γ values of (a) $\sim 20 \pm 4$ nmol cm^{-2}, (b) $\sim 140 \pm 20$ nmol cm^{-2} and (c) $\sim 420 \pm 70$ nmol cm^{-2} (determined from CV measurements), produced by depositing for times of (a) 5, (b) 30, and (c) 100 s, respectively, for a constant potential of −1.1 V. Note the linearity of the amount of $Ni(OH)_2$ deposited with the deposition time.

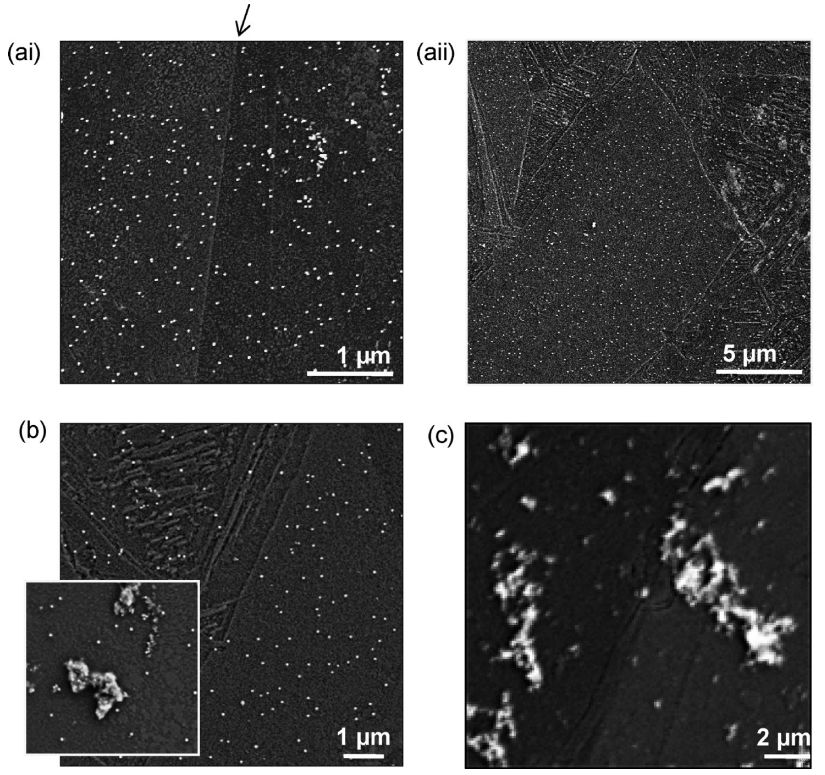

Figure 2. Typical FE-SEM images obtained from $Ni(OH)_2$ deposited pBDD electrodes for (a) $\Gamma \sim 20$ nmol cm^{-2} (images i and ii are obtained at higher and lower resolution, respectively) (b) $\Gamma \sim 140$ nmol cm^{-2}, and (c) $\Gamma \sim 420$ nmol cm^{-2}. Deposition times (at −1.1 V versus Ag/AgCl) were 5, 30, and 100 s, respectively. The inset to panel (b) is 2.5 μm x 2.5 μm.

dx.doi.org/10.1021/jp109526b |J. Phys. Chem. C XXXX, XXX, 000–000

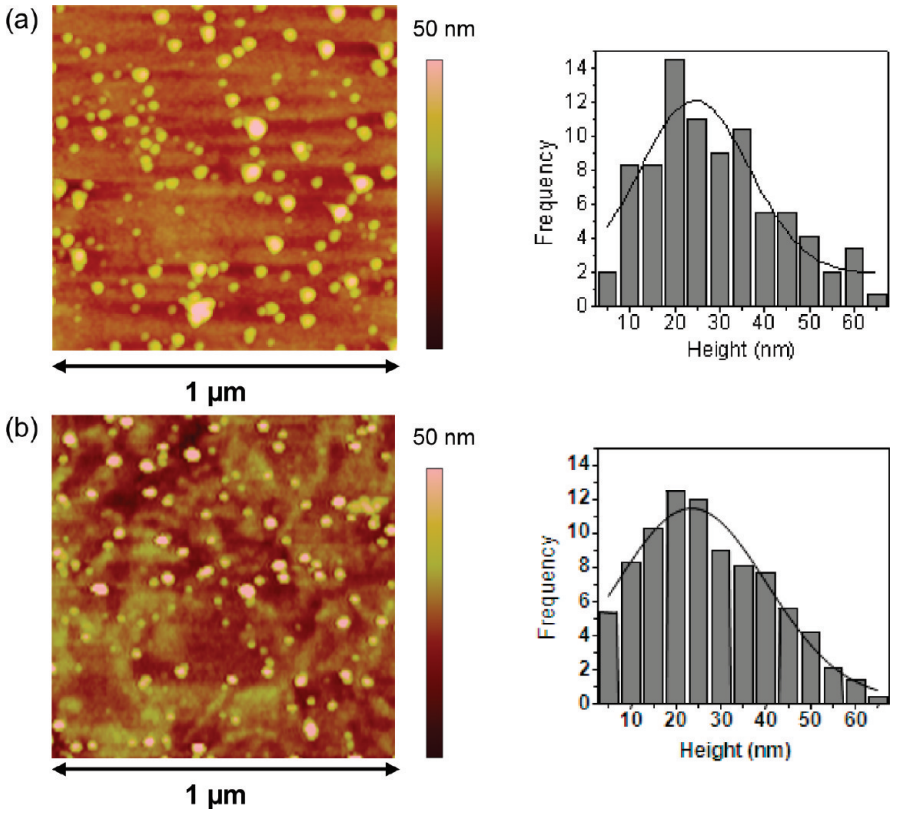

Figure 3. AFM (tapping mode) 1 μm × 1 μm height images of $Ni(OH)_2$ deposited onto a pBDD electrode on two differing conductivity grains (distinguished by height differences from differential polishing) for $\Gamma \sim 20$ nmol cm^{-2} (5 s deposition). Opposite each is a histogram showing NP height distribution.

At the shortest deposition times (Figure 2ai), the FE-SEM images show isolated NPs that are distributed uniformly over the pBDD surface, even though pBDD is a heterogeneous surface comprising grains (crystal faces) of varying conductivity (due to differential boron uptake).[25] Two grains are evident in Figure 2a; the grain boundary is indicated by the black arrow. Figure 2aii shows that NP deposition is random over larger surface areas comprising many grains. Significantly, this contrasts with the direct metal deposition approach on pBDD, where typically the resulting approximately micrometer-sized metal nucleation structures are observed to be grain-dependent.[9,20,23,29]

Clearly, the direct route, described here, is thus much better for the production of uniformly dispersed $Ni(OH)_2$ NPs on a pBDD surface. At 30 s (Figure 2b), isolated NP deposition is still favored, but there is evidence of some aggregation, as shown in the inset. After 100 s, these aggregates appear to be larger and more numerous, although again with no preference for particular grains on the surface.

AFM was used to provide quantitative information on NP size. Figure 3 shows typical 1 μm × 1 μm AFM images for Γ $(Ni(OH)_2) \sim 20$ nmol cm^{-2} (deposition time 5 s) recorded on different pBDD grains. These were identified topographically using AFM (from larger scans) from differences in surface height. Different BDD crystallographic orientations polish at different rates, resulting in 2−6 nm steps on the surface separating differently orientated grains.[25] The associated histograms show no significant differences in NP size or number density between different grains in agreement with the FE-SEM images (Figure 2). The average NP number density from Figure 3a and b is ∼87 ± 12 and 85 ± 12 NPs μm^{-2}, respectively, and the corresponding mean NP size (taken from the AFM height data) is ∼25 ± 6 and 24 ± 6 nm, with the associated size distribution shown in the histograms. It is important to note that the close spacing of the $Ni(OH)_2$ NPs means that on the time scale of typical amperometric or voltammetric electrocatalytic measurements, with these electrodes, there will be considerable or essentially total diffusional overlap between neighboring particles.

Figure 4 shows AFM images for different $Ni(OH)_2$ deposition times of (a) 1; (b) 15; (c) 30, and (d, e) 100 s. NPs of 12 ± 3, 39 ± 9, and 43 ± 8 nm in height were found for 1, 15, and 30 s, respectively, clearly showing that the mean size of particles increases with deposition time. For 1 and 15 s, the surface coverage of NPs on the surface was 25 ± 5 NPs μm^{-2} and 87 ± 15 NPs μm^{-2}. For times of 30 s and longer, the images show signs of particle aggregation, making it difficult to quantify number densities accurately. For example, in the insert to Figure 4c, it is possible to observe discrete aggregates, although at 30 s, these are sparsely deposited over the surface, consistent with the FE-SEM data shown in Figure 2b.

After 100 s, AFM images (Figure 4d and e) show that areas of the surface have become covered with aggregated $Ni(OH)_2$ structures that are micrometers in length, similar to those seen in Figure 2c. Figure 4d is recorded on the surface of an aggregate, whereas Figure 4e, imaged over a larger length scale, shows the typical size of an aggregate, the dimensions of which are clearly shown in the cross section data (Figure 4f).

dx.doi.org/10.1021/jp109526b |J. Phys. Chem. C XXXX, XXX, 000–000

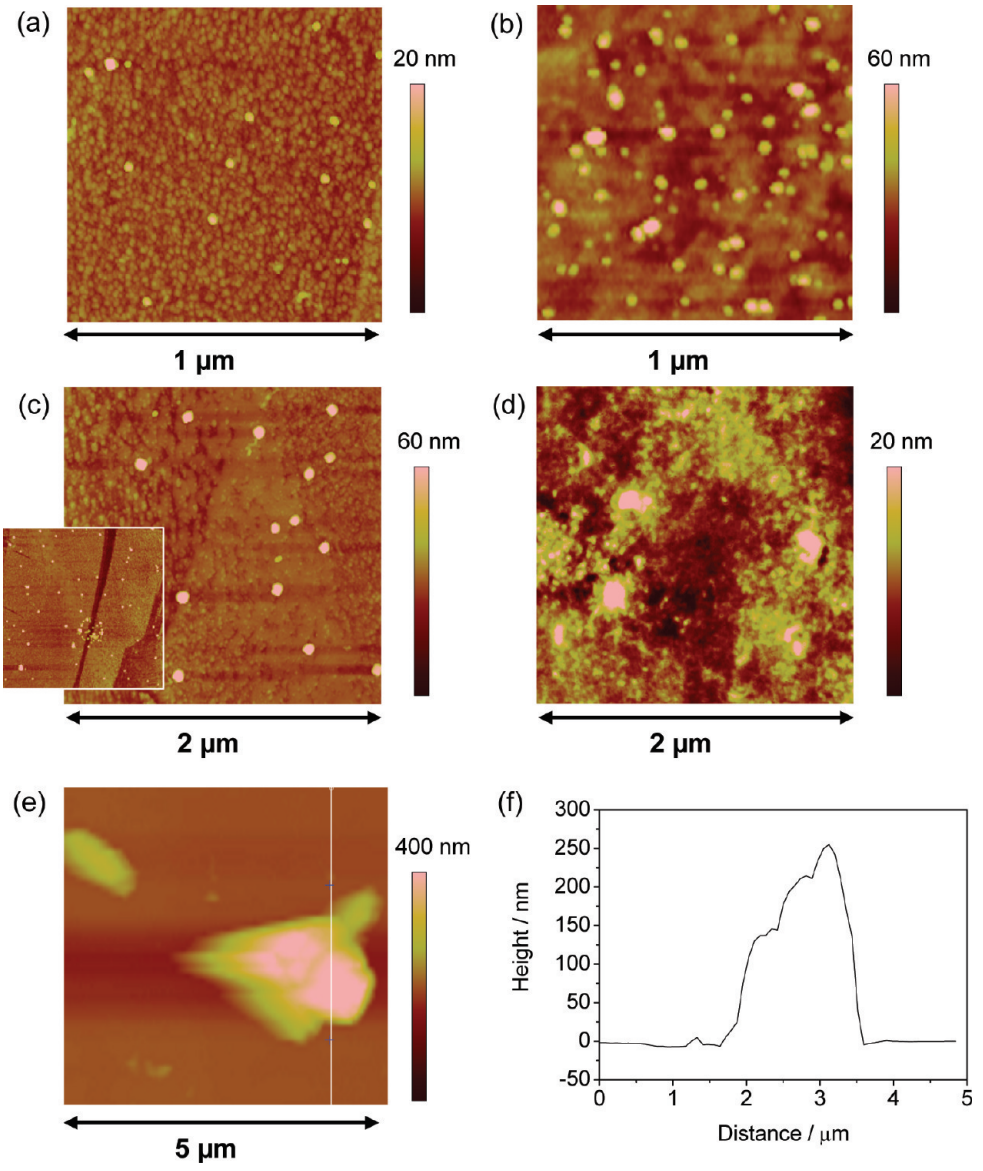

Figure 4. AFM (tapping mode) height images of $Ni(OH)_2$ deposited onto a pBDD electrode for (a) 1, (b) 15, (c) 30, and (d, e) 100 s. The insert to panel c is a 5 μm × 5 μm image. For d, the image was recorded in the area of an aggregated structure, and e was recorded with a larger scan size to emphasize the height of a typical aggregate. Part f shows a height cross section of the aggregate.

Assuming the NPs are spherical, which is likely, given their formation route (described in eq 1), AFM images (e.g., Figures 3 and 4) also enable a charge, Q_{AFM}, to be calculated associated with NP surface coverage. For example, for $\Gamma \sim 20$ nmol cm^{-2} (5 s deposition), assuming a NP surface coverage of ~86 NP μm^{-2}, Q_{AFM} is given by

$$Q_{AFM} = \frac{4\pi r^3 N_d A \rho n F}{3M} \quad (6)$$

where r is the radius of a spherical NP; N_d is the number density of NPs (surface coverage); and M and ρ are the molar mass and density of the $Ni(OH)_2$ NP particle: 92.7 g mol^{-1} and 4.15 g cm^{-3}, respectively, and $n = 1$.[30] The calculated value of $Q_{AFM} = 19 \pm 6$ μC (from eq 5) agrees well with 15.9 μC $\pm$ 4 μC obtained from consideration of Q_{ox} and Q_{red}, indicating that all NPs on the surface are electrochemically active and that the redox process involves essentially complete conversion of $Ni(OH)_2$ to Ni(OOH) in the NP.

XPS Studies. The chemical identity of the surface of the modified electrode was investigated using XPS. Figure 5 shows the XPS spectrum for a pBDD $Ni(OH)_2$-modified electrode for a deposition time of 30 s. A main peak at 855.7 eV is observed for Ni $2p_{3/2}$, with satellite peaks due to plasmon losses and final state effects at 861.5 eV.[31] By comparing the data with previous XPS studies on Ni, NiO, NiOOH, and $Ni(OH)_2$, the main peak can be assigned to Ni^{2+} in $Ni(OH)_2$.[32−34] The presence of Ni metal, NiOOH, or NiO would be indicated by peaks and satellite peaks at lower binding energies, which are not observed. Hence, under the experimental conditions employed here, it is clear that $Ni(OH)_2$ is formed predominantly via the pathway described in eq 1, resulting in NP formation in solution, followed by deposition on the electrode surface.

Electrogenerated Hydroxide Concentration Profiles. Given the proposition of homogeneous $Ni(OH)_2$ NP formation

dx.doi.org/10.1021/jp109526b |J. Phys. Chem. C XXXX, XXX, 000–000

in solution, it is informative to calculate the nickel hydroxide supersaturations, defined here as a relative saturation ratio, S,

$$S = [Ni^{2+}][OH^-]^2/K_{sp} \quad (7)$$

that are generated using the protocol outlined. $[Ni^{2+}]$ = 10 mM, and K_{sp} is known; hence, by calculating $[OH^-]$, it is possible to calculate S, using eq 7. To provide an estimate, we assume that the current that flows during electrodeposition is due to OH^- production and not Ni deposition. This is reasonable, given the results presented above. A typical current−time curve recorded during a 5 s deposition is shown in Figure 6a. It can be seen that after a short time, a relatively constant current prevails, which corresponds to a constant flux of $[OH^-]$ at the electrode surface. Under these constant flux conditions, $[OH^-]$ profiles can be calculated using the analytical expression[35]

$$C - C_0 = \frac{j_0 l}{D}\left\{\frac{Dt}{l^2} + \frac{3x^2 - l^2}{6l^2} - \frac{2}{\pi^2}\sum_m^{\infty}\frac{(-1)^m}{m^2}\exp(-Dm^2\pi^2 t/l^2)\cos\frac{m\pi x}{l}\right\} \quad (8)$$

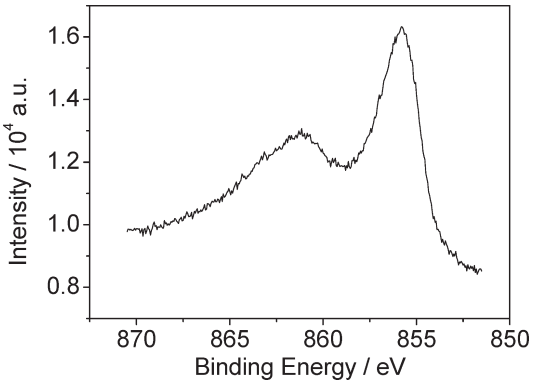

Figure 5. XPS Ni $2p_{3/2}$ spectra of $Ni(OH)_2$ modified pBDD electrode with deposition parameters of −1.1 V for 30 s.

where C is the concentration, C_0 is the initial concentration; j_0 is the flux obtained from $j_0 = \bar{i}/(nF)$, where $\bar{i}$ is the experimental current density measured during deposition; D is the diffusion coefficient of hydroxide ions (= 5.6×10^{-5} cm^2 s^{-1}),[36] l is the separation between the electrode surface and a parallel boundary (here, we use l = 0.22 cm so that diffusion from or to the electrode surface is unrestricted), t is time, x is the distance from electrode, and m is the number of points used (= 100) in the numerical simulation.

Concentration profiles have been simulated for three different times: t = 1, 5, and 15 s (lower, middle, and upper ▲ data points, respectively), indicative of the time scales employed herein. It can be seen that $>10^{-4}$ M concentrations of hydroxide are generated close to the electrode, which when converted using eq 7 into S values (○ in Figure 6), produce very high values, on the order of 10^5−10^6. Thus, it is no surprise that using this precipitation approach,[24] homogeneous NPs of nickel hydroxide are produced.

Although the electrogeneration of $[OH^-]$ may occur differently at the different electrically conducting grains in pBDD, the small grain size compared with the hydroxide concentration boundary layer thickness (Figure 6) means that these grain heterogeneities will be largely unimportant. This is evidenced by the lack of grain-dependent nickel hydroxide deposition morphology, as seen in Figures 2−4.

In summary, the XPS, AFM, and FE-SEM data demonstrate that simply by changing the time scale of the deposition process, it is possible to tune and control the type of $Ni(OH)_2$ nanostructure formed on the pBDD surface, from isolated NPs of height ∼10 nm (at short times) toward larger isolated NPs and, finally, to a surface dominated by aggregated NP structures. Importantly, in these studies, we create extremely high supersaturations to favor NP formation via precipitation.[24] Furthermore, and in contrast to all other studies, we use much shorter times for $[OH^-]$ electrogeneration to prevent significant NP aggregation in solution and on the surface. This ability to readily control the size of nanostructures on a surface is valuable in the context of understanding optimal structures for electroanalysis or electrocatalysis, which we focus on in the remainder of this paper.

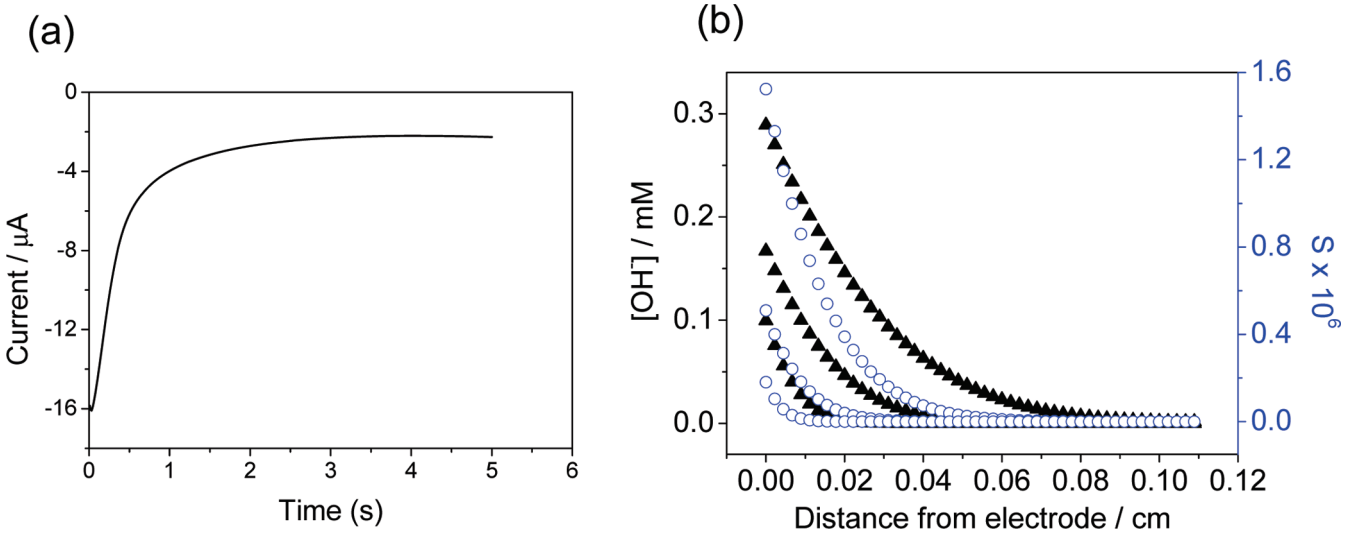

Figure 6. (a) Typical current−time curve recorded by holding the pBDD electrode at −1.1 V for 5 s in a solution containing 10 mM $Ni(NO_3)_2$. (b) Numerical simulation for generation of OH^- (▲) as a function of distance from the electrode surface for times of 1 s (lower curve), 5 s (middle curve), and 15 s (upper curve). Also shown are the corresponding plots of S (○), calculated using eq 7 versus distance from electrode surface.

dx.doi.org/10.1021/jp109526b |J. Phys. Chem. C XXXX, XXX, 000–000

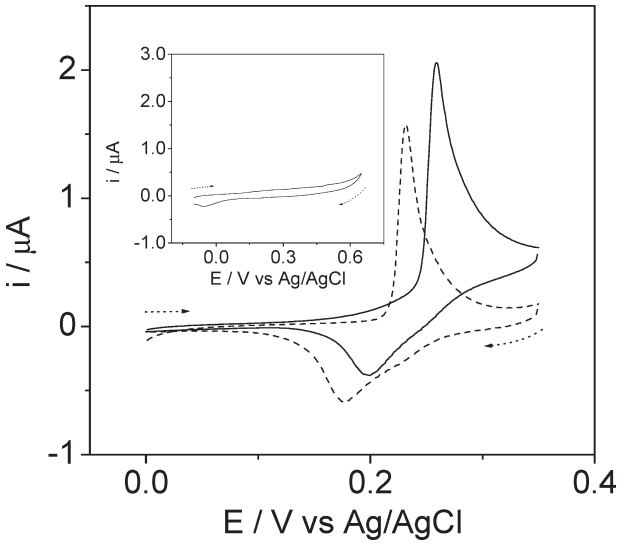

Figure 7. Cyclic voltammetry recorded in the absence (- - -) and presence (——) of 100 μM glucose, in 0.1 M KOH, for a nickel hydroxide-modified ($\Gamma \sim 20$ nmol cm^{-2}) pBDD. The scan rate is 5 mV s^{-1}. Inset: CV of the bare pBDD in 0.1 M KOH solution containing 1 mM of glucose.

Nickel Hydroxide Electrocatalyzed Glucose Oxidation. Although research on the electrochemical detection of glucose is widely reported, most studies deal with the use of the enzyme glucose oxidase to indirectly determine the concentration of glucose.[37−39] Modification of the electrode surface with a suitable electrocatalytic system to enable direct oxidation of glucose represents an interesting alternative to conventional enzymatic sensing. Recently, the use of the Ni^{2+}/Ni^{3+} redox couple to electrocatalyze glucose oxidation[40,41] has been recognized, stimulating research into the use of nickel and nickel hydroxide-/oxide[18b]-modified electrodes in strongly alkaline solutions as electrodes for glucose oxidation.

Figure 7 shows CVs of $Ni(OH)_2$ modified pBDD electrodes (——), $\Gamma \sim 20$ nmol cm^{-2}, for the oxidation of 100 μM glucose in 0.1 M KOH. The surface was uniformly covered with $Ni(OH)_2$ NPs (Figures 2a and 3). Also shown is the voltammetric response (- - -) of the surface in the absence of glucose; that is, 0.1 M KOH only. Finally, the inset gives the CV response in the presence of 1 mM glucose at *bare* pBDD. All CVs were recorded at 5 mV s^{-1}. At the bare pBDD surface, no signal was detected for the direct oxidation of glucose, even when the concentration was increased to 1 mM. This indicates that pBDD is an excellent electrochemically inert support for the nickel hydroxide NPs in alkaline glucose solutions. Other support electrodes employed previously (e.g., Au) have been shown to contribute to glucose oxidation, complicating the interpretation of the CV response.[42]

In the absence of glucose, as the potential is scanned more positive, the current increases due to oxidation of Ni^{2+} to Ni^{3+}. Figure 7 shows that in the presence of glucose, there is a clear increase in the anodic current and a decrease in the cathodic current compared with the response without glucose, as expected for an electrocatalytic process. In the potential region 0.15−0.25 V, there appears to be a small prewave that is likely to be due to the oxidation of $Ni(OH)_2$ to Ni(OOH). Beyond this potential, the current rises steeply due to the increased turnover of glucose driving the oxidation of $Ni(OH)_2$ to Ni(OOH), which is reconverted to $Ni(OH)_2$ in the process.

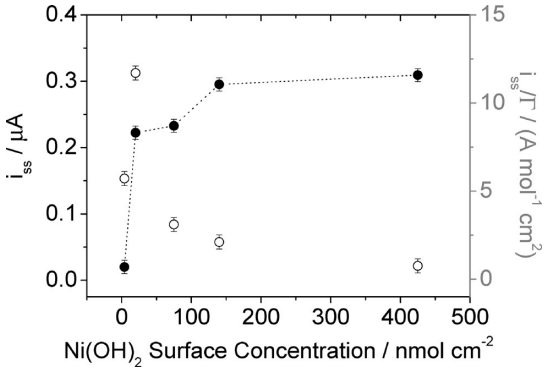

Figure 8. Electrocatalytic steady-state current for the oxidation of 100 μM glucose at nickel hydroxide-functionalized pBDD electrodes in 0.1 M KOH for Γ values (−●−) of ∼4, 20, 75, 140, and 420 nmol cm^{-2}. Normalized steady-state currents as a function of Γ, (−○−), for the same surface coverages as above.

To verify how the amount of nickel hydroxide on the surface affects the electrocatalytic response, five electrodes were prepared with differing Γ values: (a) ∼4 nmol cm^{-2} (1 s deposition; Figure 4a), (b) ∼20 nmol cm^{-2} (5 s deposition; Figures 2a and 3), (c) ∼75 nmol cm^{-2} (15 s deposition; Figure 4b), (d) ∼140 nmol cm^{-2} (30 s deposition; Figures 2b and 4c), and (e) ∼420 nmol cm^{-2} (100 s deposition; Figures 2b and 4d, e, f). For all electrodes, the current−time response for the oxidation of 100 μM glucose was recorded at 0.35 V for a period of 90 s. Although the current after this period of time approaches steady-state behavior, the true steady-state current, i_{ss}, was determined on a reciprocal time plot ($t^{-1/2}$) by extrapolating the current value to the steady-state value.

Figure 8 shows i_{ss} (●) and i_{ss}/Γ (○) as a function of Γ. Increasing Γ leads to an increase in i_{ss}, until it approaches an almost steady value for $\Gamma > 140$ nmol cm^{-2}. When i_{ss} is normalized by Γ, there is, rather strikingly, an interesting size dependence of the NP current density, which indicates that the smallest NPs (∼12 nm) are less active than those which are larger (∼25 nm). Thereafter, as the NP size increases, the effective efficiency decreases because the reaction becomes increasing mass-transport-controlled and the flux to increasingly large NPs decreases (vide infra).

For the limiting currents measured, it is useful to estimate, using eq 9, the thickness of the established diffusion layer to determine whether the reaction is under kinetic or mass transfer control.

$$i_{ss} = nFADC/\delta \qquad (9)$$

D, C, and δ are the diffusion coefficient of glucose (6.7×10^{-6} cm^2 s^{-1});[38] concentration of glucose (100 μM); and diffusion layer thickness, respectively. This equation treats the electrode as being uniformly active, which is reasonable, given the close NP spacing (see Figures 2−4). δ is calculated to be 3050 ($\Gamma \sim 4$ nmol cm^{-2}), 274 ($\Gamma \sim 20$ nmol cm^{-2}), 262 ($\Gamma \sim 75$ nmol cm^{-2}), 206 ($\Gamma \sim 140$ nmol cm^{-2}), and 197 μm ($\Gamma \sim 420$ nmol cm^{-2}). Except for the smallest Γ value, the δ values are similar to those measured experimentally for diffusion-controlled reactions at a macroelectrode under steady-state conditions, for which the time scale is sufficient such that natural convection operates.[43]

This simple analysis suggests that for Γ values in the range 20−140 nmol cm^{-2}, the Ni^{3+} electrocatalysed oxidation of glucose

dx.doi.org/10.1021/jp109526b |*J. Phys. Chem. C* XXXX, *XXX*, 000–000

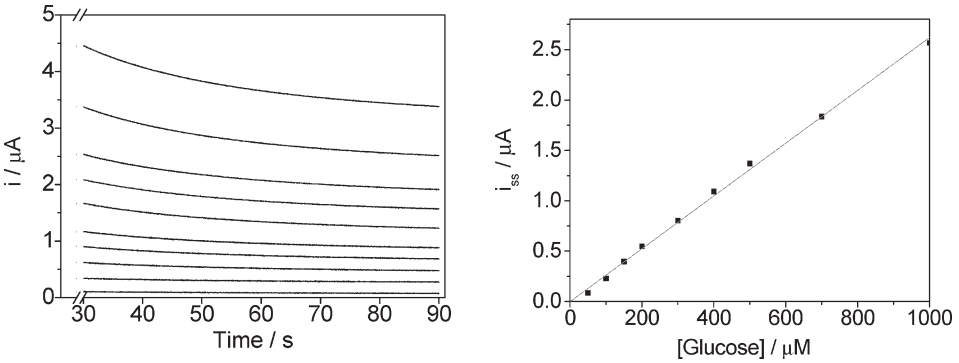

Figure 9. (a) Current−time curves recorded by holding the potential of the $Ni(OH)_2$ NP modified pBDD electrode at 0.35 V for 90 s (for Γ = 20 nmol cm^{-2}) for glucose concentrations of 0 (smallest), 50, 100, 150, 200, 300, 400, 500, 700, and 1000 μM (highest) in 0.1 M KOH. (B) Calibration curve of the steady-state current versus glucose concentration for Γ = 20 nmol cm^{-2}.

tends toward diffusion-control;[19c,44] however, the δ value calculated for Γ = 4 nmol cm^{-2} strongly suggests that other factors control the current. At this surface coverage, the NPs are the smallest, and thus, the flux to each particle is at its highest for all of the morphologies considered. Thus, the process is now likely to be under kinetic control; we are presently exploring this observation in more detail.

When considering the normalized (i_{ss}/Γ) values, (○ in Figure 8), it is clear that the isolated $Ni(OH)_2$ NP-pBDD structures formed at $\Gamma \sim 20$ nmol cm^{-2} are the most effective in terms of amount of material utilized. This highlights a key advantage of working with isolated NPs, as opposed to aggregates or thin film structures, which have been predominantly employed in previous nickel hydroxide studies.[11,12c,19c,26,27]

Figure 9a shows the $i-t$ behavior of the nickel hydroxide-modified pBDD electrode at the optimal (for material usage) $Ni(OH)_2$ surface concentration ($\Gamma \sim 20$ nM cm^{-2}) of those investigated, in 0.1 M KOH containing different glucose concentrations in the range 50 μM−1 mM. For all experiments, the potential was held at 0.35 V for a period of 90 s, although the data is shown only for times of 30−90 s to emphasize the long time behavior.

As the glucose concentration was increased, the chronoamperometric current increased monotonically. Figure 9b shows the resulting calibration curve of i_{ss} (evaluated as described above) against glucose concentration. The plot is linear, and using eq 9, the gradient yields a δ value of 230 μm, consistent with a diffusion-controlled process. From the calibration data, a sensitivity of 330 ± 10 μA mM^{-1} cm^{-2} was determined, with a limit of detection (S/N = 3) of 400 nM.

This data (especially the limit of detection) compares extremely favorably with the most sensitive nickel hydroxide modified electrode glucose sensors currently described in the literature. Reference 23 summarizes all previous studies to the year 2010. This result is particularly impressive when considering the small amount of $Ni(OH)_2$ employed on the surface (~2 μg cm^{-2}) resulting in a sensitivity based on catalyst mass of 115 ± 5 μA mM^{-1} μg^{-1}.

Catalytic Oxidation of Alcohols by Nickel Hydroxide NPs. Given the results above for glucose, $Ni(OH)_2$ NP-modified pBDD electrodes were employed to investigate the electrocatalytic oxidation of methanol and ethanol, of importance for the development of fuel cell catalysts. Alcohol electrooxidation under alkaline conditions can be achieved with higher efficiencies, making $Ni(OH)_2$ particles particularly interesting, given their stability

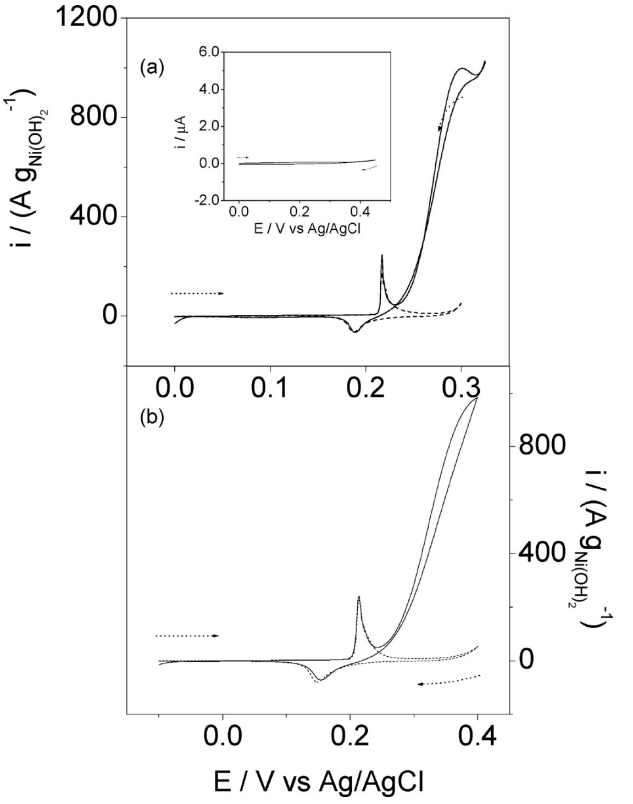

Figure 10. CVs performed at 5 mV s^{-1} at a $Ni(OH)_2$ NP modified pBDD electrode (Γ = 20 nmol cm^{-2}) in 0.1 M KOH and (a) 0.5 M ethanol and (b) 0.47 M methanol. Inset: CV of bare pBDD in a 0.1 M KOH solution containing both 1 M ethanol and 1 M methanol.

under these conditions.[45] CVs recorded in 0.1 M KOH in the absence (- - -) and presence (——) of (a) 0.5 M ethanol and (b) 0.47 M methanol, at a scan rate of 5 mV s^{-1}, are shown in Figure 10. The currents have been normalized by the mass of nickel hydroxide deposited on the electrode surface. For comparison, the inset to Figure 10a shows the response of a bare pBDD electrode in 0.1 M KOH electrolyte in the presence of both 1 M ethanol and 1 M methanol. The CV is featureless, indicating that a pBDD electrode is incapable of electrochemically oxidizing either alcohol in this potential region.

The characteristic signal of $Ni(OH)_2$ oxidation and subsequent reduction of NiOOH for the nickel hydroxide-modified

dx.doi.org/10.1021/jp109526b |J. Phys. Chem. C XXXX, XXX, 000–000

pBDD is clearly evident in the CVs in Figure 10, recorded in the absence of the alcohols. In the presence of the alcohols, the current signal rises dramatically as the electrochemically generated NiOOH is able to oxidatively catalyze the ethanol (a) and methanol (b), present in solution. Interestingly, the current that flows in the presence of the alcohol occurs at less positive potentials than many reported studies,[51,46] likely indicating that α-phase nickel hydroxide dominates.[47] This is particularly significant because it means complications from the catalytic oxidation of hydroxide ions are avoided.

Maximum normalized currents of ∼1010 A g^{-1} for ethanol (0.5 M) and ∼990 A g^{-1} for methanol (0.47 M) oxidation were found. These values are much higher than very recent reports using other nanostructured catalysts.[48,49] For example, CVs employing electrodes modified by Pt/MnO_2/carbon nanotubes (CNTs) showed a maximum catalytic current of ∼450 A g^{-1} in an electrolyte solution containing 1 M methanol in 1 M $HClO_4$.[10,48] Replacement of the Pt component of the composite by RuPt resulted in maximum currents of ∼900 A g^{-1} for the same electrolyte conditions.[9,48] In other work, CNT-modified electrodes functionalized with Pt and PtRu NPs produced normalized currents up to 300 A g^{-1} using 0.5 M H_2SO_4 as electrolyte and 1 M methanol.[49]

Although there are other reports in the literature of the use of nickel hydroxide and nickel hydroxide composite electrodes for the oxidation of methanol and ethanol,[50−54] it is not possible to extract mass-normalized catalytic current from such data for comparison with ours. The electrodes were typically prepared by electrodepositing nickel for hundreds of seconds and then oxidizing in alkaline solution to produce nickel hydroxide; the amount of nickel hydroxide on the electrodes is not typically known.

However, by noting parameters presented in these papers[50−54] (such as the anodic peak current (charge) of the nickel hydroxide modified electrodes in the absence of alcohol (provides an estimation of the amount of nickel hydroxide), the maximum electrocatalytic current obtained in a region where there are no complications from hydroxide catalyzed oxidation, and the alcohol concentration and the electrolyte employed), it is possible to draw the following qualitative conclusions: (1) The nanostructured nickel hydroxide pBDD electrode presented herein appears to show the largest electrocatalytic current based on mass usage. This re-emphasizes again one of the advantages of using $Ni(OH)_2$ isolated NP structures. (2) The larger electrocatalytic currents are achieved at lower alcohol concentrations and at less positive potentials than many of the reported studies.[46,51] (3) The deposition method employed in this work has the advantage of ease of use and is inexpensive.

CONCLUSIONS

The electrosynthesis of uniformly dispersed nickel hydroxide NPs with narrow size distributions on pBDD electrodes has been demonstrated for the first time. This was achieved by electrogenerating OH^- in the presence of Ni^{2+} to create highly supersaturated ($S > 10^5$) nickel hydroxide solutions close to the electrode for short periods of time (approximately seconds). This resulted in the electrodeposition of nickel hydroxide NPs via precipitation directly on the electrode surface, as confirmed by XPS, FE-SEM, and AFM. The size of the NPs could be tuned by controlling the reaction conditions, particularly the [OH^-] electrogeneration time. After 1 s, NPs with dimensions of 12 ± 3 nm were produced with a surface coverage of 25 ± 5 NPs μm^{-1}, increasing in size and surface coverage to ∼39 ± 9 nm and 87 ± 15 NPs μm^{-2}, respectively, after 15 s. Longer times resulted in larger particles, which ultimately formed aggregates. After 100 s, the surface was dominated by such structures which were a few micrometers in height.

The nickel hydroxide surface coverage was calculated by considering the charge passed during direct oxidation of nickel hydroxide. This value was in good agreement with that calculated on the basis of AFM images of the surface coverage, assuming spherical NPs. The close correlation of the two results suggests that during this solid-state electrooxidation process, the entire volume of nickel hydroxide was oxidized, not just the surface of the NP.

The effect of NP size on electrocatalytic activity was investigated by measuring the steady-state current for the oxidation of glucose in alkaline media. It was found that for NPs ≥ 25 nm in size, glucose oxidation was predominantly diffusion-controlled. However, for the smallest NPs produced (∼12 nm) the currents passed were much smaller than expected on the basis of diffusion control; this was attributed to kinetic limitations. For glucose, the optimal surface coverage was $\Gamma \sim 20$ nmol cm^{-2}, which corresponded to isolated NPs of size ∼25 ± 6 nm and a surface coverage of 85 ± 12 NPs μm^{-2}. For the size of the electrode employed (1 mm diameter disk), this corresponded to 15 ng of nickel hydroxide on the surface. For glucose oxidation, this electrode showed a sensitivity of 330 $\mu A\ mM^{-1}\ cm^{-2}$ and a limit of detection of 400 nM. The latter represents one of the lowest limits of detection for glucose for nickel hydroxide-based electrodes.

The electrocatalytic oxidation of this electrode toward methanol and ethanol was also found to be very efficient, achieving very high density currents of ∼1010 A g^{-1} for 0.5 M ethanol and 990 A g^{-1} for 0.47 M methanol.

AUTHOR INFORMATION

Corresponding Author

*E-mail: j.macpherson@warwick.ac.uk.

Author Contributions

⊥Both authors contributed equally to this work.

ACKNOWLEDGMENT

M.V. thanks the Conselho Nacional de Desenvolvimento Científico e Tecnológico (CNPq), case award 200261/2008-8, for financial support. L.A.H. and A.N.P. acknowledge the support of EPSRC (Analytical Fund EP/F064861/1) and EPSRC/BAE Systems (Mr. David Hankey), respectively, for the award of an EPSRC Industrial Case Studentship. Some of the equipment used in this work was obtained through the Science City Advanced Materials and Hydrogen Energy project with support from Advantage West Midlands and the European Regional Development Fund. We would additionally like to thank Element Six Ltd. for the provision of high-quality pBDD samples. We are grateful to Louise Bailey and Wojciech Linhart from the Department of Physics, University of Warwick, and to Dr. Danny Law of the Daresbury Laboratory, Cheshire, U.K., for their assistance with the XPS measurements.

REFERENCES

(1) For example, see: (a) Li, H.; Li, H.; Deng, J. F. *Catal. Today* **2002,** *74*, 53. (b) Bond, G. C.; Thompson, D. T. *Catal. Rev. Sci. Eng.*

1999, *41*, 319. (c) Daniel, M. C.; Astruc, D. *Chem. Rev.* **2004,** *104*, 29. (d) Burda, C.; Chen, X.; Narayan, R.; El-Sayed, M. A. *Chem. Rev.* **2005,** *105*, 1025.

(2) (a) Vassal, N.; Salmon, E.; Fauvarque, J. F. *J. Electrochem. Soc.* **1999,** *146*, 20. (b) SacEpee, N.; Palacin, M. R.; Beaudoin, B.; Delahaye-Vidal, A.; Jamin, T.; Chabre, Y.; Tarascon, J. M. *J. Electrochem. Soc.* **1997,** *144*, 3896. (c) Chen, J.; Bradhurst, D. H.; Dou, S. X.; Liu, H. K. *J. Electrochem. Soc.* **1999,** *146*, 3606.

(3) Schäfer, H. J.; Schneider, R. *Tetrahedron* **1991,** *47*, 715.

(4) Berger, R. J.; Doesburg, E. B. M.; van Ommen, J. G.; Ross, J. R. H. *Apply. Catal. A.* **1996,** *143*, 343.

(5) Selman, J. R. In *Assessment of Research Needs for Advanced Fuel Cells by The DOE Advanced Fuel Cell Working Group (AFCWG)*; Penner, S.S. Ed.; Permagon Press: New York, 1984.

(6) (a) Cox, P.; Pletcher, D. J. *J. Appl. Electrochem.* **1990,** *20*, 549. (b) Lo, L. X.; Hwang, B. J. *J. Electrochem. Soc.* **1995,** *142*, 445. (c) Pletcher, D. J. *J. Appl. Electrochem.* **1984,** *14*, 403.

(7) Welch, C. W.; Compton, R. G. *Anal. Bioanal. Chem.* **2006,** *384*, 601.

(8) Polsky, R.; Gill, R.; Kaganovsky, L.; Willner, I. *Anal. Chem.* **2006,** *78*, 2268.

(9) Hutton, L.; Newton, M. E.; Unwin, P. R.; Macpherson, J. V. *Anal. Chem.* **2009,** *81*, 1023.

(10) (a) Jeevanandam, P.; Koltypin, Y.; Gedanken, A. *Nano Lett.* **2001,** *1*, 263–266. (b) Pejova, B.; Kocareva, T.; Najdoski, M.; Grozdanov, I. *Appl. Surf. Sci.* **2000,** *165*, 271. (c) Vidotti, M.; Salvador, R. P.; Córdoba de Torresi, S. I. *Ultrason. Sonochem.* **2009,** *16*, 35. (d) Wang, Y.; Zhu, Q. S.; Zhang, H. G. *Chem. Commun.* **2005,** *41*, 5231. (e) Liu, L.; Li, Y.; Yuan, S. M.; Ge, M.; Ren, M. M.; Sun, C. S.; Zhou, Z. *J. Phys. Chem. C.* **2010,** *114*, 251. (f) Needham, S. A.; Wang, G. X.; Liu, H. K. *J. Power Sources* **2006,** *159*, 254. (g) Duan, G. T.; Cai, W. P.; Luo, Y. Y.; Li, Z. G.; Lei, Y. *J. Phys. Chem. B* **2006,** *110*, 15729. (h) Tai, Y. L.; Teng, H. S. *Chem. Mater.* **2004,** *16*, 338.

(11) Vidotti, M.; Córdoba de Torresi, S. I. *Electrochim. Acta* **2009,** *54*, 2800.

(12) (a) Wu, M.−S.; Hsieh, H.−H. *Electrochim. Acta* **2008,** *53*, 3427. (b) Al-Ghamdia, A. A.; Mahmouda, W. E.; Yaghmoura, S. J.; Al-Marzoukia, F. M. *J. Alloys Compd.* **2009,** *486*, 9. (c) Sawaby, A.; Selim, M. S.; Marzouk, S. Y.; Mostafa, M. A.; Hosny., A. *Phys. B* **2010,** *405*, 3412.

(13) Walter, E. C.; Murray, B. J.; Favier, F.; Kaltenpoth, G.; Grunze, M.; Penner, R. M. *J. Phys. Chem. B* **2002,** *106*, 11407.

(14) Compton, R. G.; Foord, J. S.; Marken, F. *Electroanalysis* **2003,** *15*, 1349.

(15) Xu, J. S.; Granger, M. C.; Chen, Q. Y.; Strojek, J. W.; Lister, T. E.; Swain, G. M. *Anal. Chem.* **1997,** *69*, A591.

(16) Shin, D.; Tryk, D. A.; Fujishima, A.; Merkoci, A.; Wang, J. *Electroanal.* **2005,** *17*, 305.

(17) (a) Therese, G. H. A.; Kamath, P. V. *Chem. Mater.* **2000,** *12*, 1195. (b) Tan, Y.; Srinivasan, S.; Choi, K.-C. *J. Am. Chem. Soc.* **2005,** *127*, 3596. (c) Streinz, C. C.; Hartman, A. P.; Motupally, S.; Weidner, J. W. *J. Electrochem. Soc.* **1995,** *142*, 1084.

(18) (a) Giovanelli, D.; Lawrence, N. S.; Jiang, L.; Jones, T. G. J.; Compton, R. G. *Sens. Actuators, B* **2003,** *88*, 320. (b) Reim, R. E.; Van Effen, R. M. *Anal. Chem.* **1986,** *58*, 3203.

(19) (a) Deo, R. P.; Lawrence, N. S.; Wang, J. *Analyst* **2004,** *129*, 1076. (b) Huang, J. F. *Chem. Commun.* **2009,** *10*, 1270. (c) Jafarian, M.; Forouzandeh, F.; Danaee, I.; Gobal, F. *J. Solid State Electrochem.* **2009,** *13*, 1171–1179. (d) Abdel Rahim, M. A.; Abdel Hameed, R. M.; Khalil, M. W. *J. Power Sources* **2004,** *134*, 160.

(20) Stradiotto, N. R.; Toghill, K. E.; Xiao, L.; Moshar, A.; Compton, R. G. *Electroanalysis* **2009,** *21*, 2627.

(21) Chang, Y.; Qiao, J.; Liu, Q.; Shangguan, L.; Ma, X.; Shuang, S.; Dong, C. *Anal. Lett.* **2008,** *41*, 3147.

(22) Toghill, K. E.; Xiao, L.; Stradiotto, N. R.; Compton, R. G. *Electroanalysis* **2010,** *22*, 491.

(23) Toghill, K. E.; Xiao, L.; Phillips, M. A.; Compton, R. G. *Sens. Actuators, B* **2010,** *147*, 642.

(24) Sangwal, K. *Additives and Crystallisation Processes: From Fundamentals to Applications*; John Wiley & Sons Ltd: West Sussex, U.K., 2007.

(25) Wilson, N. R.; Clewes, S. E.; Newton, M. E.; Unwin, P. R.; Macpherson, J. V. *J. Phys. Chem. B* **2006,** *110*, 5639.

(26) Corrigan, D. A.; Knight, S. L. *J. Electrochem. Soc.* **1987,** *134*, 377.

(27) Portemer, F.; Delahaye-Vidal, A.; Figlarz, M. *J. Electrochem. Soc.* **1992,** *139*, 671.

(28) *Handbook of Chemistry and Physics*, 90th ed.; Lide, D. R., Ed.; CRC Press: Boca Raton, FL, 2009.

(29) Colley, A. L.; Williams, C. G.; Johansson, U. D.; Newton, M. E.; Unwin, P. R.; Wilson, N. R.; Macpherson, J. V. *Anal. Chem.* **2006,** *78*, 2539.

(30) Torto, N.; Ruzgas, T.; Gorton, L. *J. Electroanal. Chem.* **1999,** *454*, 252.

(31) Grosvenor, A. P.; Biesinger, M. C.; Smart, R. St. C.; McIntyre, N. S. *Surf. Sci.* **2006,** *600*, 1771.

(32) Deki, S.; Hosokawa, A.; Beleke, A. B.; Mizuhata, M. *Thin Solid Films* **2009,** *517*, 1546.

(33) Chigane, M.; Ishikawa, M. *J. Chem. Soc., Faraday Trans.* **1998,** *94*, 3665.

(34) McIntyre, N. S.; Cook, M. G. *Anal. Chem.* **1975,** *47*, 2008.

(35) Crank, J. *The Mathematics of Diffusion*, 2nd ed.; Clarendon Press: Oxford, UK, 1975.

(36) Breiter, M.; Hoffmann, K. *Z. Elektrochem.* **1960,** *64*, 462.

(37) Wang, J. *Electroanal.* **2001,** *13*, 983.

(38) Newman, J. D.; Turner, A. P. F. *Biosens. Bioelectron.* **2005,** *20*, 2435.

(39) Burt, D. P.; Unwin, P. R. *Electrochem. Commun.* **2008,** *6*, 934.

(40) Cheung, K.-C.; Wong, W.-L.; Ma, D.-L.; Lai, T.-S.; Wong, K.-Y. *Coord. Chem. Rev.* **2007,** *251*, 2367.

(41) Quintino, M.; Winnischofer, H.; Nakamura, K.; Araki, K.; Toma, H. E.; Angnes, L. *Anal. Chim. Acta* **2005,** *539*, 215.

(42) (a) Casella, I. G.; Guascito, M. R.; Sannazzaro, M. G. *J. Electroanal. Chem.* **1999,** *462*, 202. (b) Xiang, C.; Qing Ji, X.; Shouzhuo, Y. *Electroanalysis* **2003,** *15*, 987.

(43) Amatore, C.; Szunerits, S.; Thouin, L.; Warkocz, J.-C. *Electroanalysis* **2001,** *13*, 646.

(44) Shamsipur, M.; Najafi, M.; Hosseini, M.-R. M. *Bioelectrochemistry* **2010,** *77*, 120.

(45) See, for example, (a) Wasmus, S.; Kuver, A. *J. Electroanal. Chem.* **1999,** *461*, 14. (b) Carrete, L.; Friedrich, K. A.; Stimming, U. *ChemPhysChem.* **2000,** *1*, 164. (c) Parsons, R.; VanderNoot, T. *J. Electroanal. Chem.* **1988,** *257*, 9. (d) Villullas, H. M.; Mattos-Costa, F. I.; Bulhoes, L. O. S. *J. Phys. Chem. B* **2004,** *108*, 12898. (d) Huang, S. Y.; Chang, C. M.; Wang, K. W.; Yeh, C. T. *ChemPhysChem* **2007,** *8*, 1774. (e) Antolini, E. J. *Power Sources* **2007,** *170*, 1.

(46) (a) Zhou, C.; Wang, H.; Peng, F.; Liang, J.; Yu, H.; Yang, J. *Langmuir* **2009,** *25*, 7711. (b) Wu, B.; Hu, D.; Kuang, Y.; Liu, B.; Zhang, X.; Chen, J. *Angew. Chem. Intl. Ed.* **2009,** *48*, 4751. (c) Yi, Q.; Huang, W.; Zhang, J.; Liu, X.; Li, L. *Catal. Commun.* **2008,** *9*, 2053. (d) Weng, Y. C.; Chou, T. C. *J. Electrochem. Soc.* **2006,** *153*, H127. (e) Danaeea, I.; Jafariana, M.; Forouzandeha, F.; Gobalb, F.; Mahjania, M. G. *Int. J. Hydrogen Energy* **2008,** *33*, 4367. (f) Cox, P.; Pletcher, D. *J. Appl. Electrochem.* **1990,** *20*, 549.

(47) (a) Kim, M. S.; Kim, K. B. *J. Electrochem. Soc.* **1998,** *145*, 507. (b) Dijksma, M. W.; Notten, P. H. L. *Electrochim. Acta* **2006,** *51*, 3609.

(48) Zhou, C.; Wang, H.; Peng, F.; Liang, J.; Yu, H.; Yang, J. *Langmuir* **2009,** *25*, 7711.

(49) Wu, B.; Hu, D.; Kuang, Y.; Liu, B.; Zhang, X.; Chen, J. *Angew. Chem. Intl. Ed.* **2009,** *48*, 4751.

(50) Yi, Q.; Huang, W.; Zhang, J.; Liu, X.; Li, L. *Catal. Commun.* **2008,** *9*, 2053.

(51) El-Shafei, A. A. *J. Electroanal. Chem.* **1999,** *471*, 89.

(52) Weng, Y. C.; Chou, T. C. *J. Electrochem. Soc.* **2006,** *153*, H127.

(53) Danaeea, I.; Jafariana, M.; Forouzandeha, F.; Gobalb, F.; Mahjania, M. G. *Int. J. Hydrogen Energy* **2008,** *33*, 4367.

(54) Cox, P.; Pletcher, D. *J. Appl. Electrochem.* **1990,** *20*, 549.